Shaped cathodes for the production of ultra-short multi-electron pulses

Ariel Alcides Petruk, Kostyantyn Pichugin, and Germán Sciaini[a)]
Department of Chemistry and Waterloo Institute for Nanotechnology, University of Waterloo, Waterloo, Ontario N2L 3G1, Canada

(Received 19 October 2016; accepted 11 January 2017; published online 25 January 2017)

An electrostatic electron source design capable of producing sub-20 femtoseconds (rms) multi-electron pulses is presented. The photoelectron gun concept builds upon geometrical electric field enhancement at the cathode surface. Particle tracer simulations indicate the generation of extremely short bunches even beyond 40 cm of propagation. Comparisons with compact electron sources commonly used for femtosecond electron diffraction are made.
[http://dx.doi.org/10.1063/1.4974779]

INTRODUCTION

The field of ultrafast structural dynamics is quickly growing, as shorter and brighter hard X-ray and electron pulses are being produced and implemented to light up atoms in motion.[1–8] The advent of forth generation light sources[9,10] has made the production of ultra-bright femtosecond (fs) hard X-ray pulses possible, which have been successfully applied for time-resolved diffraction[11–14] and ultrafast coherent imaging.[15–17] On the other hand, the use of ultrashort electron bursts has also emerged as a powerful means to atomically resolve dynamical phenomena and structure in the laboratory setting.[18–35] In this regard, different approaches for the generation of fs multi-electron bunches have been developed to meet the prerequisite time-resolution to observe the movement of atoms; i.e., sub-picosecond electron pulses and ideally the shorter the better to avoid temporal blurring in stroboscopically recorded images. Compact femtosecond electron diffraction (FED) instruments with electrostatic electron guns, based on quasi-flat cathode and anode electrodes, have enabled a time-resolution of ≅100 fs (rms, root-mean-square deviation) with bright multi-electron pulses.[36,37] For simplicity, electron pulses were assumed to be Gaussian in shape, and therefore a conversion factor of 2.355 has been used to calculate fwhm (full-width-at-half-maximum) from rms values. Recent designs with a minimal cathode-to-sample distance have brought the temporal resolution of these sources closer to the limit imposed by their initial energy spread—or single electron pulse limit.[30,38–41] Electron kinetic energies (*KE*) produced by electrostatic guns typically range from sub 1 keV to 100 keV and are commonly referred to as sub-relativistic. More advanced electron sources based on radio frequency (RF) photo-injectors are known to generate ultrashort bright pulses of relativistic electrons ($KE > 1$ MeV). This technology is relatively mature within the accelerator community due to its use in synchrotron and free electron laser facilities and has become popular for monitoring ultrafast structural dynamics.[42–49] As its energy spread gets under control, laser-driven electron acceleration is also arising as a low-cost alternative for the generation of ultrashort and ultrabright electron pulses with *KE* in the 200 keV–1 GeV range.[50–53] In addition, different active and passive electron pulse compression schemes have been proposed and/or demonstrated.[27–29,53–64] One of the most successfully applied methods in recent FED experiments with ultrabright electron bursts relies on the use of an RF (or microwave) cavity that acts

[a)]Author to whom correspondence should be addressed. Electronic mail: gsciaini@uwaterloo.ca

as a temporal lens.[27–29,55,56,60–63] This methodology was found to compress dense sub-relativistic multi-electron pulses down to 67 fs (rms).[60] Shorter multi-electron pulses are expected from this approach for which synchronization noise has limited the instrument response to about 80–150 fs (rms).[60–62] However, a recent phase-lock scheme based on passive optical enhancement has reduced this timing jitter to only ≅5 fs (rms).[65–67] Therefore, RF pill-lens electron pulse rebunching still holds great promise in providing sub-20 fs (rms) temporal resolution with bright multi-electron bunches.[56] Furthermore, all-optical electron pulse compression throughout the use of a single cycle THz resonator has recently shown to bring the duration of multi-electron pulses from 395 fs (rms) to 32 fs (rms) [930 fs (fwhm) to 75 fs (fwhm)] with minimal long-term timing drift ≅ 4 fs (rms).[68,69] This method is expected to generate even shorter multi-electron bursts.[68]

RESULTS AND DISCUSSION

Here, we introduce a rather simple all-electrostatic electron gun design that delivers multi-electron bursts as short as 12 fs (rms) [28 fs (fwhm)] at a relatively long electron propagation distance of 10 cm (sample position in our instrument) without the need of electron pulse temporal rebunching. A 300 kV FED setup based on this source concept is under construction at the University of Waterloo. The electron gun exploits the advantage of strong on-axis electric field acceleration at the electron birth. Figure 1 shows a computer-aided design (CAD) of the key electron source components alongside a geometrical depiction of the photocathode head. The cathode surface has a parabolic shape with a small flat circular area of 1 mm in diameter centered at the symmetry axis or electron propagation axis defined as $(0, 0, z)$. This flat region is necessary to avoid an excessive kick in the transverse direction acting on off-axis electrons that greatly deteriorates the transverse and longitudinal properties of the electron bunch. The cathode is positioned inside a double magnetic lens (in-lens system). The magnetic fields generated by each lens point in the opposite direction along the z-axis in order to provide a resultant field $B_z = 0$ at the cathode surface (0, 0, 0). This is a necessary condition to null emittance growth caused by magnetic fields at the electron pulse birth.[70] This in-lens source design yields a lateral spot size ≅ 190 μm (rms) for a quasi-parallel electron beam at the sample's plane. A normalized transverse emittance of 0.025 mm mrad (or transverse coherence length of about 3 nm)

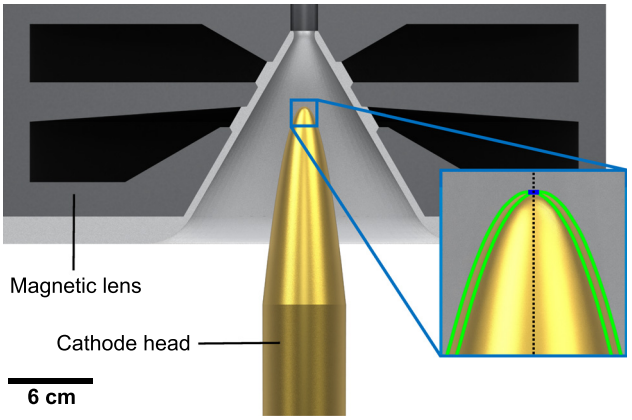

FIG. 1. CAD of the electron source concept. The main components are a parabolically shaped photocathode head with a small flat region and a double magnetic lens system with a conical inner form. This cathode shape has been carefully selected in order to confer an on-axis geometrical surface electric field magnitude of 50 MV/m without exceeding a maximum of 60 MV/m in other parts of the head. The in-lens system ensures $B_z = 0$ at the electron birth to avoid magnetic emittance growth. The conical anode shape helps to maintain the surface electric field at the anode $|E_a| \lesssim 5$ MV/m and brings the magnetic poles closer to the cathode head. The magnetic lens system has been optimized in order to obtain, within practical constraints, a reasonable electron spot size at the sample position and low power consumption to avoid water-cooling. Inlet: black dotted line corresponds to the symmetry z-axis; green curves depict two parabolas displaced from the propagation axis by 0.5 mm in the radial direction and which follow the equation $f(r) = 1.6\ \text{cm}^{-1}\ \text{r}^2$; blue segment highlights the flat region of 1 mm in diameter.

was obtained. This value suffices for the study of most inorganic and organic crystalline materials composed of small molecules. The lens system has been optimized to operate under the assumption of a core material with a relative magnetic permeability of 10^4 and a saturation magnetic field of 1.5 T. Such values are easily attainable by various soft magnetic iron alloys.[71] The required total power was estimated to be only 200 W.

Local electric field enhancement by several orders of magnitude ($\cong$1 GV/m) is a well-known effect in field emitters and single electron to a few electrons photo-triggered tip sources.[72–78] Recently, such nanoemitters have been successfully applied to monitor photocurrents in nanostructures[77] as well as ultrafast structural dynamics.[78] The introduced cathode head exploits the use of moderate geometrical field enhancement while permitting the generation of multi-electron bunches.

Electrons in simulations were generated at the cathode surface considering a temporal (longitudinal) Gaussian profile of 6 fs (rms) [14 fs (fwhm)], an initial energy spread of 0.2 eV, and a lateral (transverse) Gaussian spot size of 50 μm (rms). Such initial electron pulse parameters can be obtained via single-photon photoemission using the second harmonic from the output of a non-collinear optical parametric amplifier (NOPA).[79–81] A NOPA provides the frequency tunability necessary to match the work function of various metal candidates such as Ti, stainless steel, Mo, and W. The photocathode is held at a potential $V = -300$ kV with respect to ground. The cathode-anode separation distance along the propagation axis, $d_z \cong 5$ cm, confers an average on-axis electric field $\langle E_z \rangle = -\frac{\Delta V}{d_z} \cong -6$ MV/m. Equipotential lines, calculated using Poisson Superfish,[82] are shown in panel A of Fig. 2 (red traces). A large increase in the magnitude of the on-axis electric field $|E_z|$ can be observed as we approach the cathode head reaching a maximum value of 50 MV/m at the surface, see Fig. 2(b).

One of the major concerns of the current design is vacuum breakdown that can compromise the stability of our electron source. Critical surface vacuum breakdown fields, $E_{s,c}$, have been measured and found to be $E_{s,c} \cong 6.5 - 10$ GV/m for refractory metals.[83–85] Such critical threshold is commonly expressed as $|E_{s,c}| = \beta_m \beta_g |\Delta V_c|/d$, where β_m and β_g are microscopic and geometrical field enhancement factors, respectively, and ΔV_c is the critical applied potential drop over a given separation distance, d, between two electrodes. Thus, $|\Delta V_c|/d$ equals the magnitude of the average critical applied field $|\langle E_c \rangle|$, and $\beta_g |\langle E_c \rangle|$ becomes what we refer to as the "geometrical critical surface electric field" $|E_{g,c}|$, which therefore results in $|E_{s,c}| = \beta_m |E_{g,c}|$. Typical values of β_m for polished surfaces lie in the range of 100–300 (with 100 corresponding to mirror-like surface finishing[85]). On the other hand, the magnitude of the maximum geometrical surface electric field $|E_{g,max}|$ in previous compact electron gun designs was calculated to be about 20 MV/m and therefore satisfies the condition $\beta_m |E_g| < |E_{s,c}|$. Note that we cannot modify $|E_{s,c}|$ but β_m and $|E_g|$ within certain limits with $\beta_m \to 1$ for a roughness free surface.

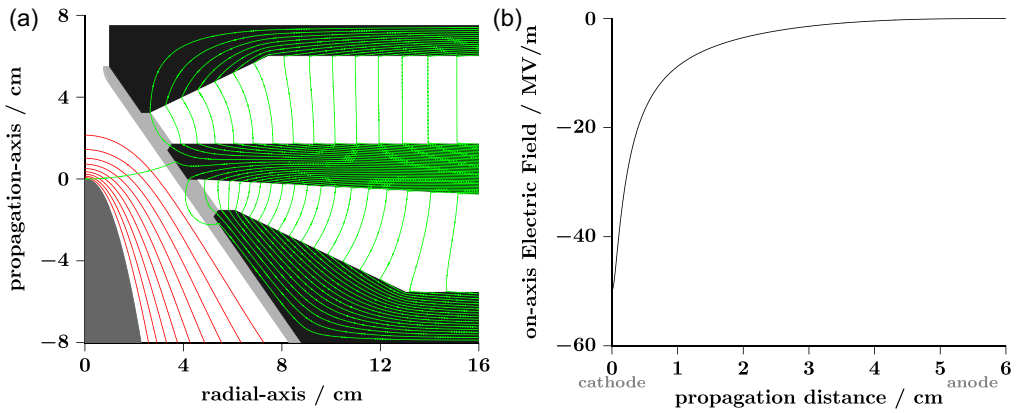

FIG. 2. (a) Schematic of the electron source concept. Equipotential and magnetic field lines are shown in red and green, respectively. (b) Electric field values obtained along the centrosymmetric axis (0, 0, z) for a cathode held at −300 kV. Calculations were done using Poisson Superfish.[82]

Surface conditioning is known to reduce dark current and greatly increase $|\langle E_c \rangle|$[86–88] by bringing β_m from several hundreds to about 20–50 for refractory metals.[84] The use of a solid cathode head made of Ti, for instance, is therefore essential to allow for proper surface processing. This is difficult to achieve in back illuminated electron guns due to the implementation of ultrathin film photocathodes that can be easily damaged by arcing. On this subject, the cathode shape was optimized to obtain a maximum geometrical surface electric field $|E_{g,max}| < 60\,\mathrm{MV/m}$ in order to maintain $\beta_m|E_g|$ below $|E_{s,c}|$. In addition, the source design ensures low surface electric fields at the anode electrode ($|E_a| \lesssim 5\,\mathrm{MV/m}$), a fact that will greatly mitigate anode-initiated vacuum breakdown.[88]

Fig. 3 shows the electron pulse duration σ_{tz} (rms) obtained from ASTRA simulations[89] for different electron source geometries as a function of the number of electrons per bunch. Black trace corresponds to our 300 kV FED electron gun concept for a total electron propagation distance $d_T = 10\,\mathrm{cm}$. Blue and red traces refer to the results obtained for conventional 100 kV compact FED setups with flat parallel electrodes, $d_T = 2\,\mathrm{cm}$, and constant on-axis electric fields of $E_z = -20$ MV/m and -10 MV/m, respectively. Note that despite the relatively long propagation distance, the proposed design provides $\sigma_{tz} < 20$ fs for bunches containing 10^4 electrons, and only $\sigma_{tz} \cong 12$ fs in the limit of low space charge effects. It should be mentioned, however, that the main disadvantage of the proposed electron source is its relatively larger spot size, $\cong 190\,\mu$m (rms), when compared with that of a compact FED setup, $\cong 55\,\mu$m (rms), with the same initial electron beam parameters.

The most noteworthy feature of this new source design is its ability for delivering ultrashort multi-electron bursts after significantly long propagation distances. As can be seen in Fig. 4(a) by direct comparison against conventional FED setups, geometrical field enhancement plays a key role in minimizing the temporal broadening caused by energy spread at

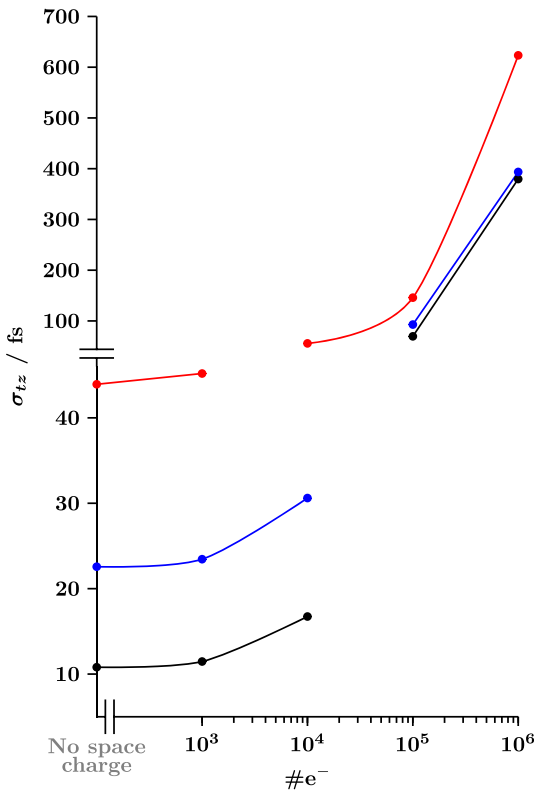

FIG. 3. Standard deviation or root-mean-square (rms) electron pulse duration (σ_{tz}, in fs) as a function of the number of electrons per bunch (#e$^-$) obtained from ASTRA particle tracer simulations.[89] Black trace corresponds to our 300 kV FED design and $d_T = 10\,\mathrm{cm}$. Blue and red traces correspond to compact 100 kV FED setups (i.e., large flat cathodes) with $d_T = 2\,\mathrm{cm}$ and constant electrostatic fields of $E_z = -20$ MV and -10 MV/m, respectively.

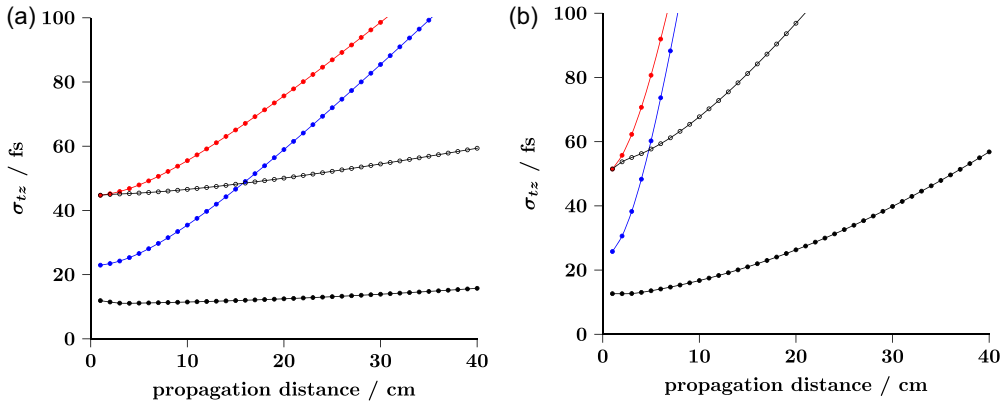

FIG. 4. Electron pulse duration σ_{tz} (rms) as a function of propagation distance from the cathode surface for bunches containing 10^3 and 10^4 electrons, panels (a) and (b), respectively. Black closed dots: our 300 kV FED design. Blue and red dots: compact 100 kV FED setups with constant electric fields of $E_z = -20$ MV/m and $E_z = -10$ MV/m, respectively. Black open dots: compact 300 kV FED setup with constant electric field $E_z = -10$ MV/m.

photoemission. Temporal broadening is known to be dominant at the initial stage of electron propagation[90] and found to be, approximately, inversely proportional to the geometrical surface electric field at the electron birth. Hence, geometrical surface field enhancement appears as a simple means to reduce the temporal broadening introduced by the initial momentum spread.

Therefore, the proposed electrostatic electron source approach lessens the need of using microwave cavities to compensate for such temporal spreading.[67] Moreover, we can also observe in Fig. 4 an important decrease of the electron pulse expansion rates when *KE* is increased from 100 keV to 300 keV (red and blue dots versus closed and open black dots). This is a consequence of relativistic effects that diminish space-charge repulsive forces by a factor of γ^{-3}.[91] We find remarkable (see black closed dots in Fig. 4(b)) that σ_{tz} is below 60 fs even for a pulse containing 10^4 electrons and after 40 cm of propagation. Longer propagation distances may be advantageous for improving transverse electron beam properties owing to the use of additional electron optics and apertures between the electron source and the sample.

Given the extremely short length of the produced electron bursts, we decided to explore the effect of instabilities of the power source on the instrument response time. Fluctuations of the electron gun voltage, $\sigma_{\Delta V}$, result in variations of the arrival time (t_0) of each electron pulse to the sample (or time zero jitter, σ_{t_0}). We found for our 300 kV FED design $\sigma_{t_0}/fs \cong 4 \times 10^{-2} \cdot \sigma_{\Delta V}/\text{eV} \cdot d_T/\text{cm}$. Hence, voltage drifts of 10 ppm ($\sigma_{\Delta V} = 3$ eV) and $d_T = 10$ cm translate into $\sigma_{t_0} \cong 1.2$ fs. A state-of-the-art high-voltage power supply is therefore necessary to guarantee that the overall temporal instrument response is not limited by fluctuations of the voltage source.[92]

CONCLUSIONS

We have presented an electron source that builds solely on electrostatic fields and that is capable of generating ultrashort and bright multi-electron pulses with minimal temporal degradation over long propagation distances. The main two ingredients of this electron source design are: (i) geometrical field enhancement that increases the strength of the electric field at the electron birth and therefore reduces the temporal broadening caused by initial energy spread; and (ii) higher *KE* that helps to diminish the detrimental effects of space charge and leads to a decrease of the electron pulse expansion rate. With a time resolution down to $\cong$ 12 fs (rms), FED instruments based on this new electron gun concept hold great promise in resolving even high-frequency vibrational modes without the necessity of implementing RF-electron pulse rebunching or all-optical electron pulse compression schemes.

ACKNOWLEDGMENTS

We would like to dedicate this work in honor to the memory of Professor Ahmed Zewail, who greatly contributed to our community with pioneering experiments. We thank Majed Chergui (EPFL) for providing us with the opportunity to contribute to this special issue. We acknowledge initial discussions about ASTRA code with Gustavo Moriena (University of Toronto). Funding for this project was provided by the Natural Science and Engineering Research Council of Canada and the Canada Foundation for Innovation. G.S. would like to acknowledge the support provided by the Canada Research Chair program.

[1]A. H. Zewail, "4D ultrafast electron diffraction, crystallography, and microscopy," Annu. Rev. Phys. Chem. **57**, 65–103 (2006).
[2]K. J. Gaffney and H. N. Chapman, "Imaging atomic structure and dynamics with ultrafast x-ray scattering," Science **316**, 1444–1448 (2007).
[3]M. Chergui and A. H. Zewail, "Electron and x-ray methods of ultrafast structural dynamics: Advances and applications," ChemPhysChem **10**, 28–43 (2009).
[4]G. Sciaini and R. J. D. Miller, "Femtosecond electron diffraction: Heralding the era of atomically resolved dynamics," Rep. Prog. Phys. **74**, 096101 (2011).
[5]F. Carbone, P. Musumeci, O. J. Luiten, and C. Hebert, "A perspective on novel sources of ultrashort electron and X-ray pulses," Chem. Phys. **392**, 1–9 (2012).
[6]M. Hada, K. Pichugin, and G. Sciaini, "Ultrafast structural dynamics with table top femtosecond hard X-ray and electron diffraction setups," Eur. Phys. J. Spec. Top. **222**, 1093–1123 (2013).
[7]R. J. D. Miller, "Femtosecond crystallography with ultrabright electrons and x-rays: Capturing chemistry in action," Science **343**, 1108–1116 (2014).
[8]T. Elsaesser and M. Woerner, "Perspective: Structural dynamics in condensed matter mapped by femtosecond x-ray diffraction," J. Chem. Phys. **140**, 020901 (2014).
[9]J. Arthur, G. Materlik, R. Tatchyn, and H. Winick, "The LCLS: A fourth generation light source using the SLAC linac," Rev. Sci. Instrum. **66**, 1987–1989 (1995).
[10]P. Emma *et al*., "First lasing and operation of an Ångstrom-wavelength free-electron laser," Nat. Photonics **4**, 641–647 (2010).
[11]A. M. Lindenberg *et al*., "Atomic-scale visualization of inertial dynamics," Science **308**, 392–395 (2005).
[12]D. M. Fritz *et al*., "Ultrafast bond softening in bismuth: Mapping a solid's interatomic potential with x-rays," Science **315**, 633–636 (2007).
[13]J. Tenboer *et al*., "Time-resolved serial crystallography captures high-resolution intermediates of photoactive yellow protein," Science **346**, 1242–1246 (2014).
[14]T. R. M. Barends *et al*., "Direct observation of ultrafast collective motions in CO myoglobin upon ligand dissociation," Science **350**, 445–450 (2015).
[15]H. N. Chapman *et al*., "Femtosecond X-ray protein nanocrystallography," Nature **470**, 73–77 (2011).
[16]A. Barty *et al*., "Self-terminating diffraction gates femtosecond X-ray nanocrystallography measurements," Nat. Photonics **6**, 35–40 (2012).
[17]L. Redecke *et al*., "Natively inhibited *Trypanosoma brucei* cathepsin B structure determined by using an x-ray laser," Science **339**, 227–230 (2013).
[18]J. C. Williamson, J. Cao, H. Ihee, H. Frey, and A. H. Zewail, "Clocking transient chemical changes by ultrafast electron diffraction," Nature **386**, 159–162 (1997).
[19]H. Ihee *et al*., "Ultrafast x-ray diffraction of transient molecular structures in solution," Science **309**, 1223–1227 (2005).
[20]B. J. Siwick, J. R. Dwyer, R. E. Jordan, and R. J. D. Miller, "An atomic-level view of melting using femtosecond electron diffraction," Science **302**, 1382–1385 (2003).
[21]P. Baum, D.-S. Yang, and A. H. Zewail, "4D visualization of transitional structures in phase transformations by electron diffraction," Science **318**, 788–792 (2007).
[22]G. Sciaini *et al*., "Electronic acceleration of atomic motions and disordering in bismuth," Nature **458**, 56–59 (2009).
[23]R. Ernstorfer *et al*., "The formation of warm dense matter: Experimental evidence for electronic bond hardening in gold," Science **323**, 1033–1037 (2009).
[24]M. Eichberger *et al*., "Snapshots of cooperative atomic motions in the optical suppression of charge density waves," Nature **468**, 799–802 (2010).
[25]P. Reckenthaeler *et al*., "Time-resolved electron diffraction from selectively aligned molecules," Phys. Rev. Lett. **102**, 213001 (2009).
[26]C. J. Hensley, J. Yang, and M. Centurion, "Imaging of isolated molecules with ultrafast electron pulses," Phys. Rev. Lett. **109**, 133202 (2012).
[27]M. Gao *et al*., "Mapping molecular motions leading to charge delocalization with ultrabright electrons," Nature **496**, 343–346 (2013).
[28]V. R. Morrison *et al*., "A photoinduced metal-like phase of monoclinic VO_2 revealed by ultrafast electron diffraction," Science **346**, 445–448 (2014).
[29]R. P. Chatelain, V. R. Morrison, B. L. M. Klarenaar, and B. J. Siwick, "Coherent and incoherent electron-phonon coupling in graphite observed with radio-frequency compressed ultrafast electron diffraction," Phys. Rev. Lett. **113**, 235502 (2014).
[30]T. Ishikawa *et al*., "Direct observation of collective modes coupled to molecular orbital-driven charge transfer," Science **350**, 1501–1505 (2015).
[31]C.-Y. Ruan, V. A. Lobastov, F. Vigliotti, S. Chen, and A. H. Zewail, "Ultrafast electron crystallography of interfacial water," Science **304**, 80–84 (2004).

[32]R. K. Raman *et al.*, "Direct observation of optically induced transient structures in graphite using ultrafast electron crystallography," Phys. Rev. Lett. **101**, 077401 (2008).
[33]N. Erasmus *et al.*, "Ultrafast dynamics of charge density waves in $4H_b$ $TaSe_2$ probed by femtosecond electron diffraction," Phys. Rev. Lett. **109**, 167402 (2012).
[34]S. Nie, X. Wang, H. Park, R. Clinite, and J. Cao, "Measurement of the electronic Grüneisen constant using femtosecond electron diffraction," Phys. Rev. Lett. **96**, 025901 (2006).
[35]D.-S. Yang, P. Baum, and A. H. Zewail, "Ultrafast electron crystallography of the cooperative reaction path in vanadium dioxide," Struct. Dyn. **3**, 034304 (2016).
[36]B. J. Siwick, J. R. Dwyer, R. E. Jordan, and R. J. D. Miller, "Ultrafast electron optics: Propagation dynamics of femtosecond electron packets," J. Appl. Phys. **92**, 1643–1648 (2002).
[37]C. T. Hebeisen *et al.*, "Grating enhanced ponderomotive scattering for visualization and full characterization of femtosecond electron pulses," Opt. Express **16**, 3334 (2008).
[38]M. Aidelsburger, F. O. Kirchner, F. Krausz, and P. Baum, "Single-electron pulses for ultrafast diffraction," PNAS **107**, 19714–19719 (2010).
[39]L. Waldecker, R. Bertoni, and R. Ernstorfer, "Compact femtosecond electron diffractometer with 100 keV electron bunches approaching the single-electron pulse duration limit," J. Appl. Phys. **117**, 044903 (2015).
[40]C. Gerbig, S. Morgenstern, C. Sarpe, M. Wollenhaupt, and T. Baumert, "Femtosecond transmission electron diffraction on single crystalline graphite," in *International Conference on Ultrafast Structural Dynamics* (2012), p. IT3D.3.
[41]C. Gerbig, A. Senftleben, S. Morgenstern, C. Sarpe, and T. Baumert, "Spatio-temporal resolution studies on a highly compact ultrafast electron diffractometer," New J. Phys. **17**, 043050 (2015).
[42]J. Yang *et al.*, "Diffractive imaging of coherent nuclear motion in isolated molecules," Phys. Rev. Lett. **117**, 153002 (2016).
[43]J. B. Hastings *et al.*, "Ultrafast time-resolved electron diffraction with megavolt electron beams," Appl. Phys. Lett. **89**, 184109 (2006).
[44]P. Musumeci *et al.*, "Multiphoton photoemission from a copper cathode illuminated by ultrashort laser pulses in an RF photoinjector," Phys. Rev. Lett. **104**, 084801 (2010).
[45]P. Musumeci, J. T. Moody, C. M. Scoby, M. S. Gutierrez, and M. Westfall, "Laser-induced melting of a single crystal gold sample by time-resolved ultrafast relativistic electron diffraction," Appl. Phys. Lett. **97**, 063502 (2010).
[46]Y. Murooka *et al.*, "Transmission-electron diffraction by MeV electron pulses," Appl. Phys. Lett. **98**, 251903 (2011).
[47]S. L. Daraszewicz *et al.*, "Structural dynamics of laser-irradiated gold nanofilms," Phys. Rev. B **88**, 184101 (2013).
[48]P. Zhu *et al.*, "Femtosecond time-resolved MeV electron diffraction," New J. Phys. **17**, 063004 (2015).
[49]S. P. Weathersby *et al.*, "Mega-electron-volt ultrafast electron diffraction at SLAC National Accelerator Laboratory," Rev. Sci. Instrum. **86**, 073702 (2015).
[50]J. Faure *et al.*, "A laser–plasma accelerator producing monoenergetic electron beams," Nature **431**, 541–544 (2004).
[51]V. Malka *et al.*, "Principles and applications of compact laser–plasma accelerators," Nat. Phys. **4**, 447–453 (2008).
[52]V. Marceau, C. Varin, T. Brabec, and M. Piché, "Femtosecond 240-keV electron pulses from direct laser acceleration in a low-density gas," Phys. Rev. Lett. **111**, 224801 (2013).
[53]S. Tokita *et al.*, "Single-shot femtosecond electron diffraction with laser-accelerated electrons: Experimental demonstration of electron pulse compression," Phys. Rev. Lett. **105**, 215004 (2010).
[54]P. M. Weber, S. D. Carpenter, and T. Lucza, "Reflectron design for femtosecond electron guns," Proc. SPIE **2521**, 23–30 (1995).
[55]L. Veisz *et al.*, "Hybrid dc–ac electron gun for fs-electron pulse generation," New J. Phys. **9**, 451 (2007).
[56]T. van Oudheusden *et al.*, "Electron source concept for single-shot sub-100 fs electron diffraction in the 100 keV range," J. Appl. Phys. **102**, 093501 (2007).
[57]G. H. Kassier, K. Haupt, N. Erasmus, E. G. Rohwer, and H. Schwoerer, "Achromatic reflectron compressor design for bright pulses in femtosecond electron diffraction," J. Appl. Phys. **105**, 113111 (2009).
[58]Y. Wang and N. Gedik, "Electron pulse compression with a practical reflectron design for ultrafast electron diffraction," IEEE J. Sel. Top. Quantum Electron. **18**, 140–147 (2012).
[59]K. P. Grzelakowski and R. M. Tromp, "Temporal and lateral electron pulse compression by a compact spherical electrostatic capacitor," Ultramicroscopy **130**, 36–43 (2013).
[60]T. van Oudheusden *et al.*, "Compression of subrelativistic space-charge-dominated electron bunches for single-shot femtosecond electron diffraction," Phys. Rev. Lett. **105**, 264801 (2010).
[61]M. Gao *et al.*, "Full characterization of RF compressed femtosecond electron pulses using ponderomotive scattering," Opt. Express **20**, 12048 (2012).
[62]R. P. Chatelain, V. R. Morrison, C. Godbout, and B. J. Siwick, "Ultrafast electron diffraction with radio-frequency compressed electron pulses," Appl. Phys. Lett. **101**, 081901 (2012).
[63]A. Gliserin, A. Apolonski, F. Krausz, and P. Baum, "Compression of single-electron pulses with a microwave cavity," New J. Phys. **14**, 073055 (2012).
[64]G. H. Kassier *et al.*, "Photo-triggered pulsed cavity compressor for bright electron bunches in ultrafast electron diffraction," Appl. Phys. B **109**, 249–257 (2012).
[65]A. Gliserin, M. Walbran, and P. Baum, "Passive optical enhancement of laser-microwave synchronization," Appl. Phys. Lett. **103**, 031113 (2013).
[66]M. Walbran, A. Gliserin, K. Jung, J. Kim, and P. Baum, "5-femtosecond laser-electron synchronization for pump-probe crystallography and diffraction," Phys. Rev. Appl. **4**, 044013 (2015).
[67]A. Gliserin, M. Walbran, F. Krausz, and P. Baum, "Sub-phonon-period compression of electron pulses for atomic diffraction," Nat. Commun. **6**, 8723 (2015).
[68]C. Kealhofer *et al.*, "All-optical control and metrology of electron pulses," Science **352**, 429–433 (2016).
[69]A. Ryabov and P. Baum, "Electron microscopy of electromagnetic waveforms," Science **353**, 374–377 (2016).
[70]M. Reiser, *Theory and Design of Charged Particle Beams*, 2nd ed. (Wiley-VCH, 2008).
[71]D. C. Jiles, *Introduction to Magnetism and Magnetic Materials*, 2nd ed. (CRC Press, 1998).

[72]P. Hommelhoff, Y. Sortais, A. Aghajani-Talesh, and M. A. Kasevich, "Field emission tip as a nanometer source of free electron femtosecond pulses," Phys. Rev. Lett. **96**, 077401 (2006).
[73]C. Ropers, D. R. Solli, C. P. Schulz, C. Lienau, and T. Elsaesser, "Localized multiphoton emission of femtosecond electron pulses from metal nanotips," Phys. Rev. Lett. **98**, 043907 (2007).
[74]R. Bormann, M. Gulde, A. Weismann, S. V. Yalunin, and C. Ropers, "Tip-enhanced strong-field photoemission," Phys. Rev. Lett. **105**, 147601 (2010).
[75]A. Paarmann *et al*., "Coherent femtosecond low-energy single-electron pulses for time-resolved diffraction and imaging: A numerical study," J. Appl. Phys. **112**, 113109 (2012).
[76]J. Hoffrogge *et al*., "Tip-based source of femtosecond electron pulses at 30 keV," J. Appl. Phys. **115**, 094506 (2014).
[77]M. Müller, A. Paarmann, and R. Ernstorfer, "Femtosecond electrons probing currents and atomic structure in nanomaterials," Nat. Commun. **5**, 5292 (2014).
[78]M. Gulde *et al*., "Ultrafast low-energy electron diffraction in transmission resolves polymer/graphene superstructure dynamics," Science **345**, 200–204 (2014).
[79]G. M. Gale, M. Cavallari, T. J. Driscoll, and F. Hache, "Sub-20-fs tunable pulses in the visible from an 82-MHz optical parametric oscillator," Opt. Lett. **20**, 1562 (1995).
[80]G. Cerullo, M. Nisoli, S. Stagira, and S. De Silvestri, "Sub-8-fs pulses from an ultrabroadband optical parametric amplifier in the visible," Opt. Lett. **23**, 1283 (1998).
[81]A. Shirakawa, I. Sakane, M. Takasaka, and T. Kobayashi, "Sub-5-fs visible pulse generation by pulse-front-matched noncollinear optical parametric amplification," Appl. Phys. Lett. **74**, 2268–2270 (1999).
[82]See http://laacg.lanl.gov/laacg/services/serv_codes.phtml for Poisson Superfish.
[83]D. Alpert, "Initiation of electrical breakdown in ultrahigh vacuum," J. Vac. Sci. Technol. **1**, 35 (1964).
[84]M. Kildemo, S. Calatroni, and M. Taborelli, "Breakdown and field emission conditioning of Cu, Mo, and W," Phys. Rev. Accel. Beams **7**, 092003 (2004).
[85]P. G. Slade, *The Vacuum Interrupter: Theory, Design, and Application* (CRC Press, 2007).
[86]Y. Ito, Y. Yamano, S. Kobayashi, and Y. Saito, "Vacuum electrical breakdown characteristics and surface condition of Ti electrodes with oxidation conditions," IEEE Trans. Dielectr. Electr. Insul. **13**, 98–104 (2006).
[87]F. Le Pimpec *et al*., "Vacuum breakdown limit and quantum efficiency obtained for various technical metals using dc and pulsed voltage sources," J. Vac. Sci. Technol., A **28**, 1191 (2010).
[88]N. Nishimori *et al*., "Experimental investigation of an optimum configuration for a high-voltage photoemission gun for operation at $\geq$500 kV," Phys. Rev. Spec. Top.–Accel. Beams **17**, 053401 (2014).
[89]See http://www.desy.de/~mpyflo/ for ASTRA. A space charge tracking algorithm.
[90]V. V. Korobkin, B. M. Stepanov, S. D. Fanchenko, and M. Y. Schelev, "Pico-femtosecond electron optical photography," Opt. Quantum Electron. **10**, 367–381 (1978).
[91]T. P. Wangler, *RF Linear Accelerators*, 2nd ed. (Wiley-VCH, 2008).
[92]See http://www.heinzinger.com, Heinzinger-Electronics.